Polarimetry With a Multilayer CdTe Prototype for Soft Gamma-Ray Astrophysics

M. Moita, R. M. Curado da Silva, J. M. Maia, E. Caroli, E. Virgilli, N. Auricchio, J. B. Stephen, F. Frontera, and S. del Sordo

***Abstract*— The development of a new generation of soft gamma-ray telescopes should allow polarimetric measurements of astrophysical sources to be associated with the results from spectroscopy and imaging due to the promising developments in polarimetry achieved over the last decade. In this perspective, the advanced surveyor of transient events and nuclear astrophysics mission which includes a narrow field telescope (NFT) that comprises a wide band Laue lens (60–600 keV) associated with a high performance thick and stacked CdZnTe focal plane operating as spectrometer, imager, and scattering polarimeter has been submitted for the ESA Voyage 2050 long term scientific planning preparation. In this context, and with the aim of optimizing the focal plane configuration of an instrument such as NFT, several studies are underway. In particular, with this work we study some performance issues such as polarimeters of segmented semiconductor detectors at room temperature, such as CdZnTe and cadmium telluride (CdTe), by means of a prototype based on two planar CdTe spectroimagers operating in coincidence. The two CdTe detectors are 2-mm-thick crystals with the anode segmented in 8 × 8 pixels with 2-mm pitch. This prototype configuration allows the Compton polarimetric performance of a spectroimager to be assessed by changing the distance between the two detection layers while operating in the 100–600-keV energy range, thereby allowing the analysis of Compton polarimetry 3-D dependence. The results obtained provide relevant input to the design of large sensitive volume multilayer and 3-D sensitive focal planes.**

***Index Terms*— Compton scattering, CZT/cadmium telluride (CdTe), gamma-ray detectors, polarimetry, space instrumentation.**

Manuscript received June 30, 2021; revised September 1, 2021; accepted September 2, 2021. Date of publication September 6, 2021; date of current version November 18, 2021. This work was supported in part by the European H2020/AHEAD 2020 Project (https://ahead.iaps.inaf.it/), in part by the European Synchrotron Radiation Facility (ESRF), and in part by the Fundação para a Ciência e a Tecnologia (FCT) Fellowship under Grant PD/BD/105922/2014.

M. Moita is with the Department of Physics and Earth Science, University of Ferrara, 44122 Ferrara, Italy, and also with the LIP-Laboratório de Instrumentação e Física Experimental de Partículas, 3004-516 Coimbra, Portugal.

R. M. Curado da Silva is with the LIP-Laboratório de Instrumentação e Física Experimental de Partículas, Portugal and Physics Department, University of Coimbra, 3004-516 Coimbra, Portugal (e-mail: rui.silva@coimbra.lip.pt).

J. M. Maia is with the LIP-Laboratório de Instrumentação e Física Experimental de Partículas, Portugal and Physics Department, University of Beira Interior, 6201-001 Covilhã, Portugal.

E. Caroli, E. Virgilli, N. Auricchio, and J. B. Stephen are with the OAS of Bologna INAF Bologna, 40129 Bologna, Italy.

F. Frontera is with the Department of Physics and Earth Science, University of Ferrara, 44122 Ferrara, Italy.

S. del Sordo is with IASF-Palermo INAF Palermo, 90146 Palermo, Italy.

Color versions of one or more figures in this article are available at https://doi.org/10.1109/TNS.2021.3110472.

Digital Object Identifier 10.1109/TNS.2021.3110472

I. Introduction

SOFT gamma-ray astrophysics holds the potential of responding to many fundamental questions concerning nucleosynthesis in stellar explosions, the origin of cosmic rays, the fundamental physical processes in neutron stars and black holes [1], [2]. Over the last decade, the richness of the gamma-ray sky has been revealed through instruments on board satellites such as the International Gamma-Ray Astrophysics Laboratory (INTEGRAL) [3] or the Fermi Gamma-ray Space Telescope [4]. Furthermore, in a new era of multimessenger astronomy, joint observations of gamma-ray emission, gravitational waves, neutrinos, and cosmic rays may provide unprecedented data to locate and analyze transient sources [5], [6]. For these open scientific issues, polarimetry of high-energy sources is a key observational parameter for a better understanding of the emission mechanisms and geometry of a wide number of cosmic objects and events such as GRBs, pulsars, binary black holes, and active galactic nuclei, whose emissions are expected to be polarized. The first reliable polarization measurements in this energy range were performed by INTEGRAL [7]–[10]. More recently, the cadmium zinc telluride imager (CZTI), an instrument on board of the Indian astronomy satellite Astrosat, made the most reliable measurement, to date, of polarized hard X- to soft gamma-ray emission from the Crab pulsar and nebula in the 100–380-keV band [11]; and POLAR, a dedicated polarimeter performed the most sensitive measurements of the polarization of GRBs [12].

Our team has been developing detector prototypes for new high-energy missions exploring several configurations that could provide source emission polarimetric observations associated with spectroscopy and imaging. These prototypes, based on the cadmium telluride (CdTe) semiconductor family, were designed for coded masks and Laue lens focal plane instrument missions [13], [14]. More recently, a new mission concept has been proposed: the Advanced Surveyor of Transient Events and Nuclear Astrophysics (ASTENA). This mission concept is based on a Laue Lens gamma-ray telescope, the narrow field telescope (NFT), that is currently under development by the University of Ferrara, the Istituto di Astrofisica (INAF- Bologna and Palermo) and LIP [15], [16]. The focal plane envisaged for the NFT telescope will consist of a stack of thick detection planes (2–3-cm thickness) made with CdZnTe spectrometers with fine spatial resolution (0.3–0.5 mm) in three dimensions to guarantee both the total required high detection efficiency (>80% at 700 keV), spectroscopy response of 1% at 511 keV and the correct sampling of the point spread function (PSF) of the lens, that is of the

order of a few mm^2. The high segmentation level of the focal plane of this instrument will provide fine polarization measurements also because of the unprecedented sensitivity that can be achieved with the Laue lens focusing technique [17]. As for the use as a scattering polarimeter of a focal plane such as that of NFT, in practice, every thick (2–3 cm) layer of it can be thought of as a compact stack of a large number of thin layers (i.e., pixel detectors 0.3–0.5-mm thick). Each impinging photon that has a Compton interaction with the material can be scattered in the same incidence layer or more likely in layers at different depths as a function of the incident energy and of the scattering angle. Since the modulation produced by the initial polarization of the photon depends on the scattering angle, to evaluate the polarimetry performance of a thick detector formed by many layers it is important to study which is the actual contribution, for example in terms of counts efficiency, to the polarization evaluation of the incident photon in order to optimize the event selection criteria and, finally, to obtain the best minimum detectable polarization (MDP) level for the instrument [2]. Herein, we have used a detector comprising two CdTe pixel spectrometers, to carry out an experimental study with, in parallel, Monte Carlo simulations, to obtain information on the performance of their use as a scattering polarimeter as a function of the distance between the two layers. The distance between the two planes can be representative of a different depth of interaction of a multilayer detector such as that required for NFT. The detector envisaged for NFT and our prototype are two very different devices in terms of configuration and performance in spectroscopy and spatial resolution, while for what concerns the two constitutive materials, CZT and CdTe, from the point of view of the cross section for photons and therefore of the detection efficiency there are no relevant differences. Therefore, this study, even if carried out with a device with different characteristics, can still provide indications regarding the performance as scattering polarimeters of detectors made up of many thin layers or equivalently of segmented detectors with 3-D spatial resolution. In particular, these conclusions will contribute to the development of an optimized design of ASTENA CdTe Laue lens focal plane for polarimetric observations.

II. Compton-POLCA Prototype Experimental Setup

The Compton-POLarimetry with Cadmium telluride Array (POLCA) is composed of two aligned layers of CdTe detectors, where the distance between the two planes can be set by rotating four screws on each corner of the detector frame (Fig. 1). Each detector matrix is divided into 8×8 pixels with an area of 1.9×1.9 mm^2 each and with a 0.1-mm gap between consecutive pixels, 2-mm thick, for a total 2.31-cm^2 sensitive area. On the segmented side, the anodes are composed of Au/Ni/Au/Pt while on the crystal opposite side the cathode is made of a 300-nm-thick Pt layer as specified by the provider ACRORAD. Each detector was bonded to a PCB readout (DiClad laminate) which was fixed to an Al frame [18]. The signals generated by the 128 pixels were read by the front-end electronics based on eight eV-Products ASICs of 16 channels, [19]. Each channel consists of a charge sensitive amplifier followed by an active semi-Gaussian shaper. The signals were then processed by a custom multiparametric electronic system consisting of 128 independent channels with filters, coincidence logic and analog-to-digital converter (ADC) units. The pixel position and energy of each interaction in the detection volume were recorded for a ~40-keV energy threshold and 2-μs time coincidence window. The coincidence logic is essential to select double-event detector hits and therefore to obtain the polarized beam modulation from the double-event distribution obtained in a detector matrix plane [20]. Data were further processed and analyzed by a PC-based data acquisition (DAQ) system, which is based on a National Instruments PCI-6533 board with 32 parallel digital inputs/outputs. The DAQ was controlled by an algorithm written in LabView.

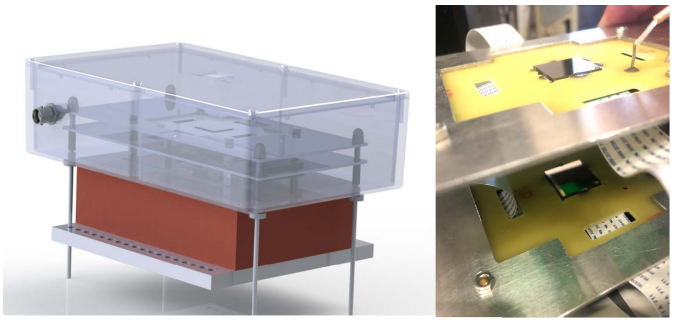

Fig. 1. Left: representation of the Compton-POLCA system with the front-end electronics enclosure (red box) and the detector enclosure (transparent) with the two detector planes inside. Right: the system allows the distance between the two detection planes to be set by tuning four screws one on each corner of the detector frame.

The Compton-POLCA prototype was tested at the high-energy diffraction and scattering beamline ID15A at the European Synchrotron Radiation Facility (ESRF), in Grenoble, France. This beamline provides ~100% polarized gamma-rays in the energy range between ~100 and ~500 keV [21]. The experimental setup inside the beamline hutch is presented in Fig. 2. In order to reduce the photon intensity to levels compatible with our DAQ system, an aluminum wedge was inserted in the beamline. The triangular shape of the wedge associated with an automated linear stage allows it to continuously reduce the beam flux up to ten orders of magnitude. After the wedge, a tungsten collimator with a variable square aperture was placed in the beam path to adjust the beam size between 0.1 and 2.0 mm. The residual scattered flux from the wedge is strongly reduced by the collimator. Furthermore, we know where the beam is impinging and its energy. This means that we know the first interaction location, therefore only scattered photons with at least one interaction in the same pixel, that have a very small area (few square mm), where the beam is impinging can create a background. The position of the wedge and the slit size were set to keep the count rate $<10^5$ counts/s. The slit sizes set were 0.2×0.2 mm^2 for 200 and 300 keV, 0.5×0.5 mm^2 for 400 keV, and 1.8×1.8 mm^2 for 500 keV. The collimated beam then reaches the Compton-POLCA which is mounted perpendicular to the beam on a five-axis motorized system: three linear stages allow movement along the x-, y- and z-directions, a rotation stage sets the movement around the z-axis, and a Eurelian cradle sets the rotation around the x-axis (Fig. 2). Through the ID15A beamline control console it was possible to manage the positioning of the linear and rotation stages, the optics hutch shutter, the wedge positioning, and the beam slit size.

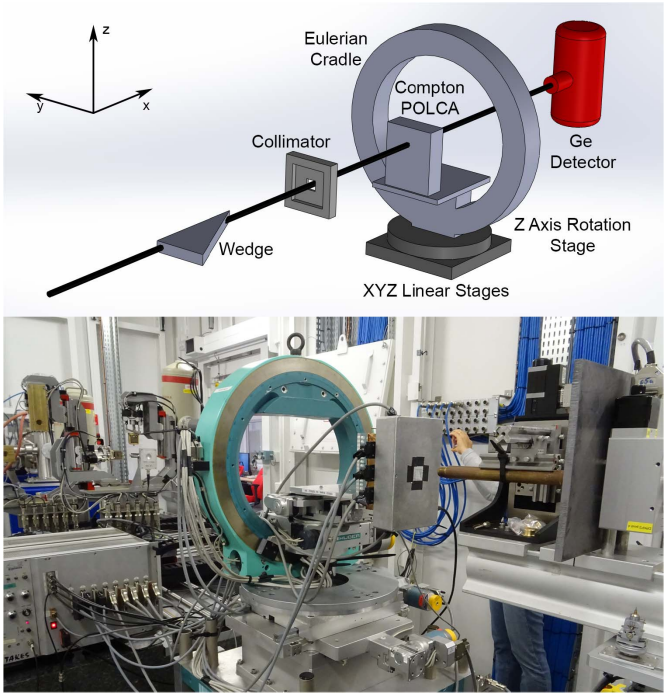

Fig. 2. Top: schematic of the main experimental setup components. Bottom: photography of the experimental setup inside the ESRF ID15A beamline hutch. The rectangular shape box, in front of the Eulerian cradle ring, contains the two-layer Compton-POLCA prototype.

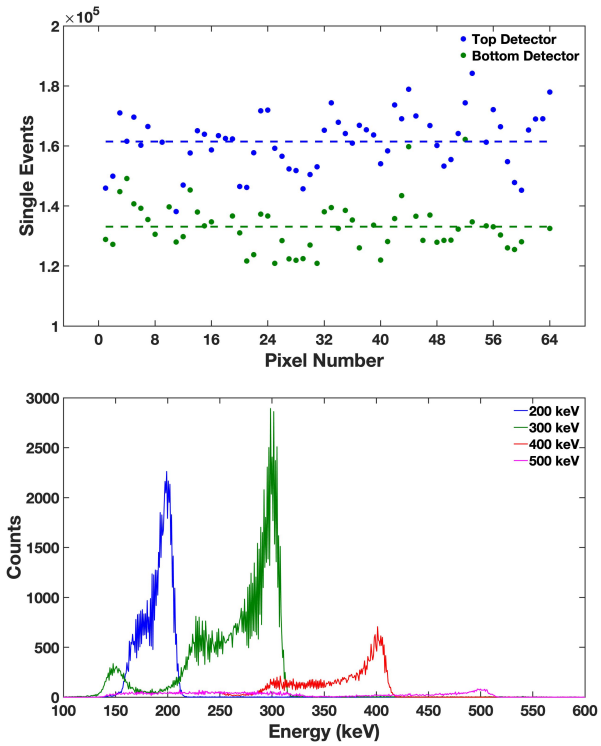

Fig. 3. Top: single events as function of the pixel number obtained from the detector pixel scans with a 300-keV beam at the ESRF for both detectors. The dotted lines are the average: bottom: 1.6013 × 10^5 single events; top: 4.1668 × 10^5 single events. Bottom: energy spectra in keV obtained for a 200-, 300-, 400-, and 500-keV beam.

During the ESRF test campaign, we performed several measurement sets by varying the beam energy (200, 300, 400, and 500 keV) and the distances between planes (8, 10, and 12 mm), aligning the beam with one of the detector central pixels. For each energy, we also performed a complete beam scan of all detector pixels, which allowed us to correct the nonuniformity of pixels' response and calibrate the energy for each pixel/channel. The recorded data were analyzed off-line by a MATLAB software custom tool that performed data processing operations prior to the polarimetric data analysis.

III. Compton Polarimetry Analysis

A. Detector Performance

Before performing the polarimetric analysis set of measurements the detectors were characterized, using the ESRF beamline and laboratory radioactive sources. By performing a complete scan of all the detector pixels we evaluated the uniformity and the spectral performance of the detector. Fig. 3 (top) presents the number of single events as a function of the pixel number obtained for both detectors. The mean value was 1.3310 × 10^5 single events for the bottom detector and 1.6146 × 10^5 for the top detector. The standard deviations are 8.5483 × 10^3 (∼6%) and 9.6266 × 10^3 (∼6%) respectively, presenting a good uniformity response. In Fig. 3 (bottom), we present the spectra obtained for the four beam energies under study. The FWHMs measured were 6.5% ± 2.3% at 200 keV, 3.9% ± 0.5% at 300 keV, 3.3% ± 0.6% @ 400 keV, and 3.9% ± 0.4% @ 500 keV.

B. Data Correction and Event Selection

To evaluate the polarimetric performance of the Compton-POLCA, we performed the matrix pixels' response nonuniformity correction [22]. Furthermore, in order to process the true double events triggered by the system and since we know the position of the first interaction, that corresponds to the position of the irradiated pixel by the collimated beam, we selected only the double events that have the first interaction in the incident pixel. This means the contribution of the background from scattering is negligible. Since the operated ID15A beam was monochromatic, we applied a further double event selection using the energy deposited in each hit validating the events for which the energy sum of the two interactions lies within a narrow energy window (1σ) centered at the selected beam energy. Multiple events were not considered in our analysis since it is not possible to determine the order of all the hits.

The dual plane configuration of the Compton-POLCA allows to sort the double events by operation mode: 1) single plane operation mode—when both interactions occur in the same plane; 2) dual plane operation mode—when the two interactions occur in different planes; and 3) full operation mode—combines the double events of the single and the dual plane modes operating simultaneously.

For each operation mode, the modulation factor was calculated from the double-event angular distribution around a central irradiated pixel, $Q_{100} = (N_{\max} - N_{\min})/(N_{\max} + N_{\min})$, where $N_{\max}$ and $N_{\min}$, are the number of double-events integrated over the two orthogonal directions defined on the detector plane along the maxima and minima of the scattered event distribution [24]–[27].

C. Polarization Modulation Analysis

The set of polarimetric measurements was dedicated to the analysis of the modulation factor as a function of interplane

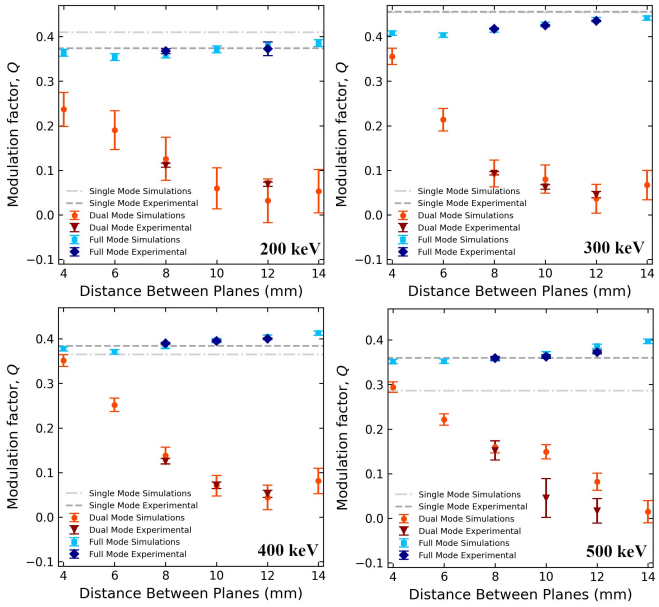

Fig. 4. Modulation factor as a function of the distance between planes for the three prototype operational modes (single, dual and full mode) and for beam energies of 200, 300, 400, and 500 keV. Single plane mode modulation (average of top and bottom planes) is represented by a straight dashed line for comparison. Both experimental and simulated curves are represented.

distance, by irradiating one of the four central pixels of the detectors setting the distance between planes at: 8, 10, and 12 mm. For each distance, the beam energy was set at: 200, 300, 400, and 500 keV. Fig. 4 shows the experimental polarimetric modulation factor obtained during the ID15A beamline measurements as well as the simulated modulation obtained for the detector prototype mass model and the experimental setup irradiation conditions, for a wider range of separations between the detection planes (4 up to 14 mm), performed with a Monte Carlo code based on MEGAlib software [23]. For each beam energy, Fig. 4 shows the modulation factor obtained for the three operation modes as a function of the distance between planes.

The single plane operation mode is independent of the distance between planes, therefore, we selected the single plane interactions of both planes and averaged the modulation factor (Fig. 4 horizontal lines). The best measured modulation factor was obtained at 300 keV for a $Q \sim 0.46$. In fact, previous polarimetric studies with single plane CdTe/CZT-based detectors with similar characteristics have shown that the best modulation factor is obtained in the energy range between 200 and 400 keV (for Q between $\sim$0.3 and $\sim$0.5) [24]–[27]. In this energy range, there is a larger fraction of Compton scattering angles close to 90°, which provide better modulation. For lower energies (<200 keV) an important fraction of double events is generated in the central pixels with a low contribution for the polarimetric modulation, since pixels are 1.9 mm × 1.9 mm and the scattered photons that escape from the irradiated pixel drops drastically to almost zero as energy decreases down to 100 keV. For higher energies (>400 keV), the average Compton scattering angle decreases, diverging from 90°, and the modulation factor drops.

In the dual plane operation mode, only the double events that are scattered in the top detector and absorbed on the bottom detector are selected. The Compton scattering angles in dual plane operation mode are on average considerably lower than the angles formed by double events in the single mode that are close to 90°. Therefore, the modulation factor in the dual plane operation mode is considerably lower ($Q \sim 0.10$ at 300 keV and 8-mm gap) than the single-mode modulation. As expected, the modulation factor shows a decrease as the distance between planes increases. As the gap between planes is increased the double events' Compton angles decrease and, therefore, the modulation decreases as well. The difference observed between the simulation and measured Q curves at 500 keV, for distances between planes >8 mm, should be associated with the larger diameter of the ESRF beam, similar to the pixel dimensions, which generate a higher ratio of peripheral double events, occurring near the pixel limits or in the neighbor pixels, that are lost and not well processed by the selection process. Furthermore, these double events are also more sensitive to system imperfections as the two planes slight misalignment ($\sim$200 μm).

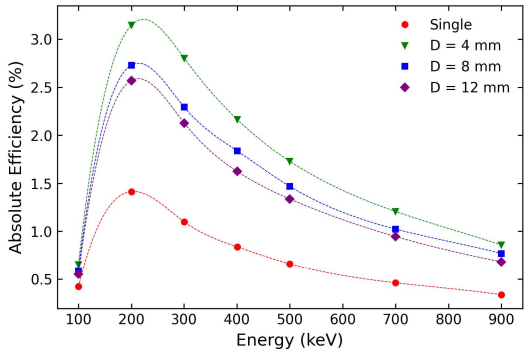

Fig. 5. Double event efficiency versus the energy, for the single plane and dual plane configurations at interplane distances (D) of 4, 8, and 12 mm. Results obtained by a Monte Carlo simulation code experimentally validated in previous research concerning double event efficiency with CdTe detectors.

When the prototype is operating in full operation mode (single and dual plane modes), the modulation factor is dominated by the contribution of the single plane mode double events for the overall modulation. A relative efficiency (normalized to the total number of triggered events) for the double events in the range of 13%–17% is measured over the 200–500-keV energy range. If we pick the precedent example at 300 keV and 8-mm gap, the modulation factor Q is $\sim$0.46 for the single plane operation mode and $\sim$0.10 for the dual plane operation mode, resulting in a combined $Q \sim 0.42$ for the full operation mode. Moreover, the trends of Fig. 4 show that the modulation factor starts by decreasing and then slightly increases with the detector interplane distance over 6-mm gap. Below 6-mm distance, the combined modulation factor decreases because the dual plane modulation decreases. Over 6 mm, the dual plane mode double events efficiency shows a decrease that can reach $\sim$50% for 12 mm (Fig. 5) and therefore this operation mode has a lower weight in the overall modulation factor. Consequently, the overall modulation tends to approach the single-layer mode modulation level, increasing slightly (between $\sim$2 and 5%) with distance up to 12 mm. Modulation curves in full detector operation mode are presented in Fig. 6 for 300 and 400 keV and an interplane distance of 8 mm. The bin angle (10°) was chosen to optimize the double-event histogram readout

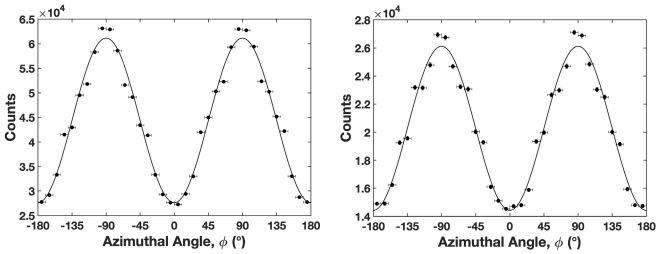

Fig. 6. Modulation curves in full detector operation mode are obtained for (left) 300 and (right) 400 keV at an interplane distance of 8 mm. The number of counts error bars are inside the dots. In order to optimize the double-event histogram readout, we applied the radial bin technique (RBT) [1], by dividing the matrix into 36 radial bins of 10° each. Pixels partially crossed by angular bin lines contribute only with a fraction of the number of events equal to the fraction of its area that is in the sector—this is an approximation since real hits inside each pixel are not uniformly distributed but have a radial dependence relative to the position of the first Compton interaction of a double-event. The modulation curve was then corrected using unpolarized data. Fit sinusoid is represented just for guideline purposes.

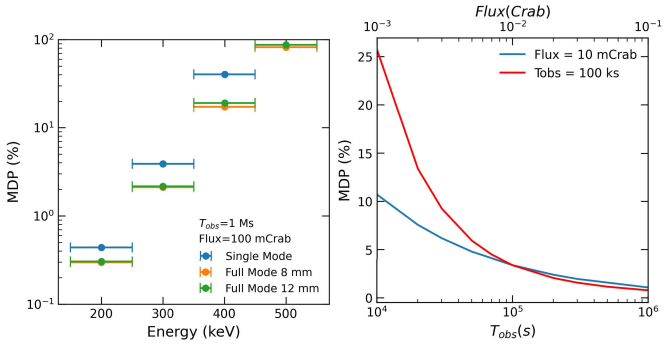

Fig. 7. Left: MDP versus energy (band energy width $\Delta E = 50$ keV) for full detector and single plane operation modes. For both cases the observation time was fixed to 1 Ms and the flux to 100 mCrab. Right: MDP in the full energy band (60–600 keV), for 100 ks, as a function of the polarized source intensity (red line) and, for 10 mCrab, as a function of the observation time (blue line).

and consequently, the measurement of the polarization angle. However, it presents a decrease of the amplitude of 5%–6% when compared to the previous data where a radial bin angle of ∼22° was used [31].

IV. NFT Focal Plane MDP

The MDP of an instrument for a given celestial source type is an essential parameter to estimate its polarimetric potential. For a space polarimeter in a background noise environment, the MDP with a 99% confidence level, is given by [28]

$$\mathrm{MDP} = \frac{4.29}{A.\epsilon.S_F.Q_{100}}\sqrt{\frac{A.\epsilon.S_f + B}{T}} \tag{1}$$

where, in the case of a focusing instruments, A is the effective area of the focusing telescope, ϵ is the double events' efficiency, S_F is the source flux over the selected energy band (photons cm^{-2} s^{-1}), B is the background noise count rate (counts/s), T is the observation time (s), and Q_{100} is the polarimetric modulation factor for a 100% polarized source.

In order to estimate the potential MDP for a broadband Laue lens telescope with the characteristics of the ASTENA NFT in a low earth orbit (LEO), we used the modulation factor Q experimentally obtained in Section III. The Compton-POLCA prototype modulation factor should be more conservative than the future NFT, however, it provides useful analysis as a function between plane distances and as a function of operation modes. As it was not possible to measure the absolute efficiencies of the various types of events during the ESRF tests with the Compton-POLCA detector due to the fact that we did not have the possibility to measure the incident photon flux, we evaluated it using a numerical model of the detection system developed in Geant4, and previously validated by laboratory measurements [22]. We defined four energy bands, with width $\Delta E = 50$ keV, centered in the four energy values we tested the Compton-POLCA. For each energy band, we integrated: the NFT effective area A, currently evaluated between 1370 and 1.764 cm^2 from 50 to 600 keV respectively, which can be computed as the product between the geometrical area of the instrument and the reflection efficiency of the lens [16]; a source flux S_f in photons/cm^2/s, and the background B in counts/s. B as a function of energy was estimated considering the background data (in counts/cm^2/s) in the 90–600-keV energy band measured by SPI/INTEGRAL in a high earth orbit and extrapolating them to the LEO, where ASTENA is proposed to be operative [29], [30]. Finally, the new estimated values for the background are integrated over the very small volume of the detector under the Laue lens PSF, resulting in a contribution that is almost more than two orders of magnitude lower with respect to the background of nonfocusing instruments. The calculated MDP is presented, in Fig. 7 (left), as a function of the energy for the single and full operation modes (distance between detector planes of 8.0 and 12.0 mm) when observing a 100-mCrab source for 1 Ms. Up to 300 keV, NFT provides fine polarimetric sensitivity, where the estimated MDP is <2%. For energies >400 keV, the estimated MDP exceeds 10%. This is explained by the decrease in the energy of the modulation factor and of the double event efficiency as well as by the decrease of the Crab flux and effective area of the NFT.

When comparing the full detector and single plane operation modes, we can observe that better MDP is obtained for the full detector operation mode. Although we measured a better modulation factor for the single plane operation mode (Fig. 4), the double event efficiency increases significantly when the two CdTe layers are closer (Fig. 5), resulting in a better MDP in full operation mode.

Finally, the MDP for a realistic cosmic point source was evaluated. For this case, both the NFT modulation factor Q and the double event efficiency were obtained by simulation using a Crab like a spectrum covering the entire Laue energy passband (60–600 keV) focused on the center of the focal plane using the Compton-POLCA mass model with an interplane distance of 8 mm. The effective area, background noise, and crab flux were integrated over the same full energy band. The results are presented in Fig. 7 (right) and show a fine polarimetric sensitivity (MDP < 5% at 99% confidence level, for a 10-mCrab source and 100-ks observation time). Furthermore, this instrument concept, based on focusing technology, will be optimized to use a large volume multilayer/3-D detectors on the focal plane. We expect that this configuration will improve the MDP at least ∼50% for the same flux and observation time, holding a promising potential to explore this new polarimetric dimension in hard X/gamma-rays astrophysics.

V. Conclusion

A Compton polarimeter prototype composed of two 2-mm-thick CdTe detectors with 8 × 8 pixels, each with 2.0-mm pitch size, was tested under a ∼100% polarized beam in the 200–500-keV energy band and for detector interplane distance ranging from 8.0 up to 12.0 mm. With these energies and gaps between planes, we obtained fine modulation factors Q of the order of ∼0.4 in full operation mode—combining single plane and dual plane operation modes. The full operational mode modulation factor consists of a combination of the single plane and dual plane modulation factors weighted by their relative efficiencies. We have observed that the modulation factor is dominated by the single plane mode double events. In particular, the relative efficiency of the dual mode events decreases rapidly with distance up to about 12 mm reaching a value of ∼25% reduction. At the same time, the dual plane modulation factor decreases while the single plane factor remains constant. In combination, this leads to a full mode modulation factor which decreases out to about 6 mm before recovering at larger distances and ending up about 2%–5% higher at 12 mm. The modulation factor behavior inferred by simulation fully agrees with that measured for the distance range where we have experimental data (from 8 to 12 mm).

As an example, for an energy of 300 keV and 8-mm gap, $Q \sim 0.46$ for the single plane mode, and $Q \sim 0.10$ in dual plane mode, for a combined $Q \sim 0.42$ in full operation mode. As can be seen, the full operation mode modulation factor is slightly lower than that for the single-layer operation, however, it is critical to operate multilayer detectors in full operation mode, since the double-events detection efficiency is maximized and consequently better MDP can be achieved.

Compton-POLCA prototype 3-D polarimetric performance provides relevant guidelines to design large sensitive volume multilayer and 3-D position sensitive focal planes. Based on these results, we have estimated the polarimetric potential of the focal plane proposed for the ASTENA NFT telescope. An MDP < 5%, at 99% confidence level, could be achievable for a 10-mCrab source and 100-ks observation time. ASTENA polarimetric performances show that such instruments hold the potential to address gamma-ray polarimetry with high sensitivity and contribute to expanding this new astrophysics knowledge window.

Acknowledgment

The authors acknowledge the European Synchrotron Radiation Facility for the provision of synchrotron radiation facilities and they would like to thank Thomas Buslaps for assistance in using beamline ID15A.

References

[1] T. Chattopadhyay, "Hard X-ray polarimetry—An overview of the method, science drivers and recent findings," 2021, *arXiv:2104.05244*. [Online]. Available: http://arxiv.org/abs/2104.05244

[2] V. Tatischeff, M. McConnell, and P. Laurent, "Gamma-ray polarimetry," in *Astronomical Polarisation from the Infrared to Gamma Rays* (Astrophysics and Space Science Library), vol. 460. 2019, pp. 109–146.

[3] N. A. Gehrels and C. Winkler, "International gamma-ray astrophysics laboratory (INTEGRAL): A future ESA mission for gamma-ray astronomy," *Proc. SPIE*, vol. 2806, pp. 210–216, Oct. 1996.

[4] A. A. Moiseev, "Gamma-ray large area space telescope: Mission overview," *Nucl. Instrum. Methods Phys. Res. A, Accel. Spectrom. Detect. Assoc. Equip.*, vol. 588, nos. 1–2, pp. 41–47, Apr. 2008.

[5] B. P. Abbott *et al.*, "Multi-messenger observations of a binary neutron star merger," *Astrophys. J. Lett.*, vol. 848, p. L12, Oct. 2017.

[6] The IceCube Collaboration, "Multimessenger observations of a flaring blazar coincident with high-energy neutrino IceCube-170922A," *Science*, vol. 361, no. 6398, p. 1378, Jul. 2018.

[7] A. J. Dean *et al.*, "Polarized gamma-ray emission from the Crab," *Science*, vol. 321, no. 5893, p. 1183, Aug. 2008.

[8] M. Forot, P. Laurent, I. A. Grenier, C. Gouiffès, and F. Lebrun, "Polarization of the Crab pulsar and nebula as observed by the *INTEGRAL*/IBIS telescope," *Astrophys. J.*, vol. 688, no. 1, p. 29, Nov. 2008.

[9] P. Laurent, J. Rodriguez, J. Wilms, M. C. Bel, K. Pottschmidt, and V. Grinberg, "Polarized gamma-ray emission from the galactic black hole Cygnus X-1," *Science*, vol. 332, pp. 438–440, Apr. 2011.

[10] D. Götz, P. Laurent, F. Lebrun, F. Daigne, and Ž. Bošnjak, "Variable polarization measured in the prompt emission of GRB 041219A using IBIS on board integral," *Astrophys. J.*, vol. 695, no. 2, pp. L208–L212, Apr. 2009.

[11] S. V. Vadawale *et al.*, "Phase-resolved X-ray polarimetry of the Crab pulsar with the AstroSat CZT imager," *Nature Astron.*, vol. 2, no. 1, pp. 50–55, 2018.

[12] S. N. Zhang *et al.*, "Detailed polarization measurements of the prompt emission of five gamma-ray bursts," *Nature Astron.*, vol. 3, no. 3, pp. 258–264, Mar. 2019.

[13] R. M. C. da Silva, E. Caroli, J. B. Stephen, and P. Siffert, "Cipher, a polarimeter telescope concept for hard X-ray astronomy," *Exp. Astron.*, vol. 15, no. 1, pp. 45–65, 2003.

[14] R. M. C. da Silva *et al.*, "Polarimetric performance study of a CZT gamma-ray burst monitor concept," *IEEE Trans. Nucl. Sci.*, vol. 53, no. 1, pp. 383–388, Feb. 2006.

[15] E. Virgilli, "The narrow field telescope on board the ASTENA mission," *Memorie Della Soc. Astron. Italiana*, vol. 90, nos. 1–2, pp. 252–255, 2019.

[16] E. Virgilli, V. Valsan, F. Frontera, E. Caroli, V. Liccardo, and J. B. Stephen, "Expected performances of a Laue lens made with bent crystals," *Proc. SPIE*, vol. 3, no. 4, 2017, Art. no. 044001.

[17] F. Frontera *et al. ESA Voyage 2050 White Paper*. Accessed: Jul. 1, 2021. [Online]. Available: http://www.cosmos.esa.int/FronteraFWhitePaperESA-voyage2050.pdf

[18] Due2Lab, Scandiano, Italia. *Detector CdZnTe*. Accessed: Jul. 1, 2021. [Online]. Available: http://www.due2lab.com/en/cdznte-detector/

[19] G. De Geronimo, P. O'Connor, A. Kandasamy, and J. Grosholz, "Advanced-readout ASICs for multielement CdZnTe detectors," *Proc. SPIE*, vol. 4784, pp. 105–118, Jan. 2003.

[20] M. Moita *et al.*, "Compton polarimetry with a multi-layer CdTe focal plane prototype," *Nucl. Instrum. Methods Phys. Res. A, Accel. Spectrom. Detect. Assoc. Equip.*, vol. 918, pp. 93–98, Feb. 2019.

[21] *ID15A—Materials Chemistry and Materials Engineering*. [Online]. Available: http://www.esrf.eu/ID15A.html

[22] R. M. C. da Silva *et al.*, "Hard X- and soft gamma-ray polarimetry with CdTe array prototypes," *IEEE Trans. Nucl. Sci.*, vol. 51, no. 5, pp. 2478–2484, Oct. 2004.

[23] A. Zoglauer. (2019). *MEGAlib—The Medium Energy Gamma-Ray Astronomy Library*. [Online]. Available: http://ascl.net/1906.018

[24] R. M. C. da Silva *et al.*, "Polarimetric performance of a Laue lens gamma-ray CdZnTe focal plane prototype," *J. Appl. Phys.*, vol. 104, no. 8, pp. 1–7, 2008.

[25] R. M. C. da Silva *et al.*, "Polarization degree and direction angle effects on a CdZnTe focal plane performance," *IEEE Trans. Nucl. Sci.*, vol. 59, no. 4, pp. 1628–1635, Aug. 2012.

[26] S. Antier *et al.*, "Hard X-ray polarimetry with Caliste, a high performance CdTe based imaging spectrometer," *Exp. Astron.*, vol. 39, no. 2, pp. 233–258, Mar. 2015.

[27] E. Caroli *et al.*, "Hard X-ray and soft gamma ray polarimetry with CdTe/CZT spectro-imager," *Galaxies*, vol. 6, no. 3, pp. 1–19, 2018.

[28] M. C. Weisskopf, E. H. Silver, H. L. Kestenbaum, K. S. Long, and R. Novick, "A precision measurement of the X-ray polarization of the Crab Nebula without pulsar contamination," *Astrophys. J.*, vol. 220, p. L117, Mar. 1978.

[29] A. J. Dean *et al.*, "The gamma-ray emissivity of the earth's atmosphere," *Astron. Astrophys.*, vol. 219, nos. 1–2, pp. 358–361, 1989.

[30] M. Khalil, F. Frontera, E. Z. I. O. Caroli, E. Virgilli, and V. Valsan, "A simulation study on the focal plane detector of the Laue project," *Nucl. Instrum. Methods Phys. Res. A, Accel. Spectrom. Detect. Assoc. Equip.*, vol. 786, pp. 59–70, Jun. 2015.

[31] M. Pinto *et al.*, "Polarimetric analysis of a CdZnTe spectro-imager under multi-pixel irradiation conditions," *Nucl. Instrum. Methods Phys. Res. A, Accel. Spectrom. Detect. Assoc. Equip.*, vol. 840, pp. 69–76, Dec. 2016.